2011 IEEE/RSJ International Conference on
Intelligent Robots and Systems
September 25-30, 2011. San Francisco, CA, USA

Soft Curvature Sensors for Joint Angle Proprioception

Rebecca K. Kramer, Carmel Majidi, Ranjana Sahai and Robert J. Wood

***Abstract*— We introduce a curvature sensor composed of a thin, transparent elastomer film (polydimethylsiloxane, PDMS) embedded with a microchannel of conductive liquid (eutectic Gallium Indium, eGaIn) and a sensing element. Bending the sensor exerts pressure on the embedded microchannel via the sensing element. Deformation of the cross-section of the microchannel leads to a change in electrical resistance. We demonstrate the functionality of the sensor through testing on a finger joint. The film is wrapped around a finger with the sensing element positioned on top of the knuckle. Finger bending both stretches the elastomer and exerts pressure on the sensing element, leading to an enhanced change in the electrical resistance. Because the sensor is soft (elastic modulus $E \sim 1$ MPa) and stretchable (>350%), it conforms to the host bending without interfering with the natural mechanics of motion. This sensor represents the first use of liquid-embedded elastomer electronics to monitor human or robotic motion.**

I. INTRODUCTION

Elastomer sheets embedded with microchannels of conductive liquid enable a rich range of electronic and sensing functionalities, with compliances not achievable by solid state devices. In contrast to rigid or flexible electronics, these liquid-embedded elastomer electronics (LE3) can be softer-than-skin and remain functional even when stretched as much as 10× their natural length (depending on the elastomer). Although LE3 cannot perform all of the same functions that are possible with conventional metals, semiconductors, and ceramics, they nonetheless exhibit an expansive range of electronic and sensing capabilities. These include stretchable wiring [1], mechanically tunable antennas [2], hyperelastic stretch [3] and pressure sensing [4], and wearable tactile arrays [5].

The most recent LE3 capability is a curvature sensor that is composed of two rectangular elastomer plates that are attached at opposite edges and at the center by a parallel strut [6]. A microchannel of conductive liquid (eutectic Gallium Indium, eGaIn) is embedded above the strut. As the plates bend, compressive force induced in the strut exerts a pressure on the embedded channel, which consequently deforms. Bending curvature is inferred from the relative change in electrical resistance of the embedded microchannel.

Position measurement and motion detection are accomplished with a combination of the elastomer-based stretch, pressure, and curvature sensors. Because the sensors are soft and stretchable, they can conform to joint rotations and will not interfere with the mechanics of body movement, for both natural and artificial systems. This mechanically passive functionality is particularly important for fingers and end effectors that perform delicate tasks and are sensitive to motion constraints. As illustrated in Fig. 1, such sensors may be incorporated into a glove to monitor hand motion or used to measure joint angles for a robotic manipulator.

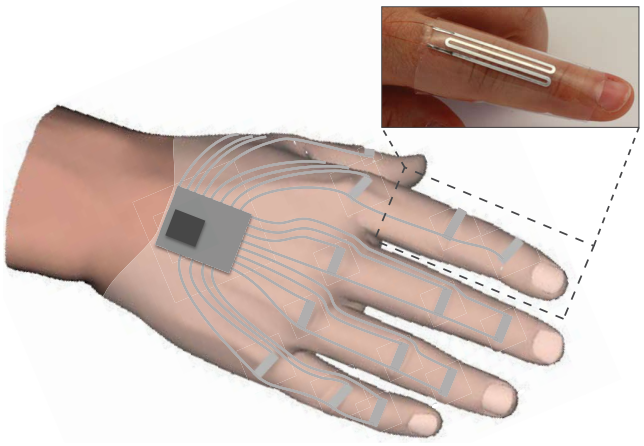

(a)

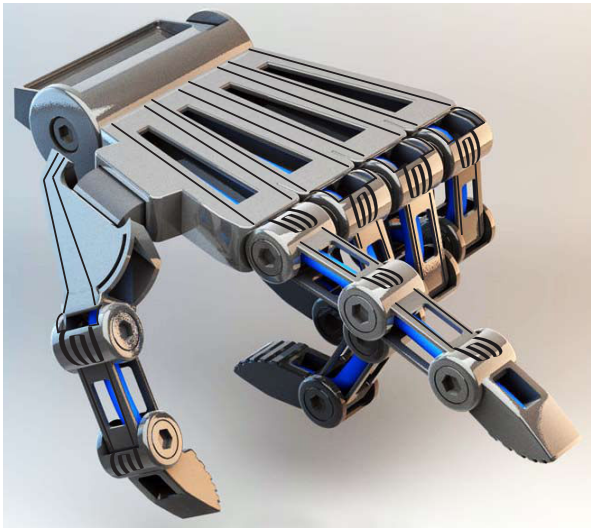

(b)

Fig. 1. Elastomer-based (LE3) curvature sensors allow mechanically non-invasive measurement of human body motion and robot kinematics. (a) An illustration of a human hand covered with curvature sensors at every joint. Inset: An actual sensor mounted on a host finger. The sensor consists of a 300 μm thick elastomer sheet embedded with a microchannel filled with a conductive fluid. (b) A concept robotic manipulator mounted with curvature sensors at the joints.

A. Previous Work

Curvature and joint angle sensors allow real-time kinematic feedback in robotic manipulation, which is necessary

The authors are with the School of Engineering and Applied Sciences, Harvard University, Cambridge, MA 02138 rkramer@fas.harvard.edu

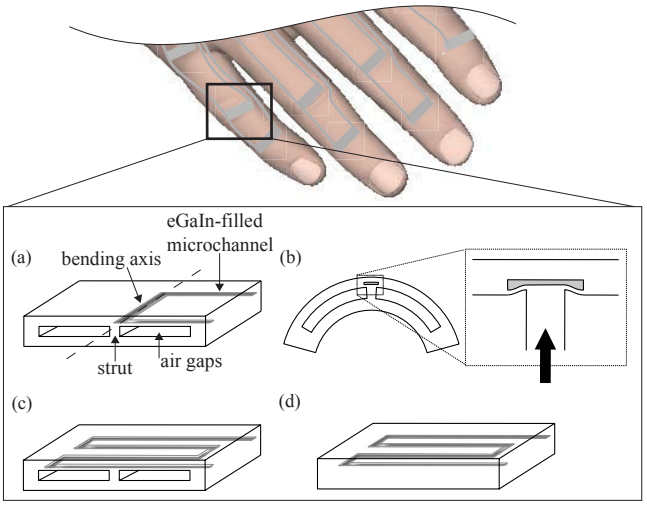

Fig. 2. Bend sensor geometries. (a) The pure curvature sensing geometry, composed of two elastomer sheets that are attached at opposite edges and at the center by a strut. A straight microchannel of conductive liquid is embedded parallel to the strut. When the sensor is bent about the axis of the strut, a compressive force is induced in the strut and applied to the embedded microchannel. As shown in (b), the cross-section of the microchannel is deformed due to the applied pressure and electrical resistance across the channel increases. (c) A serpentine channel and a perpendicular strut. When the sensor bends, the microchannel is deformed at locations where it intersects the strut. The serpentine geometry of the channel allows for simultaneous curvature and strain sensitivity. (d) An embedded serpentine microchannel. This geometry is sensitive only to strain.

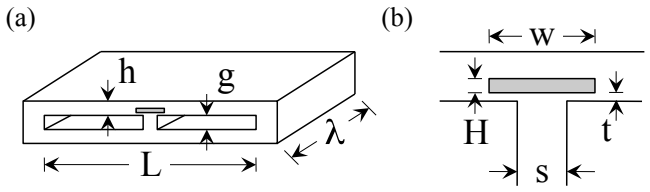

Fig. 3. Curvature sensor dimensions: h = 300 μm, g = 260 μm, L = 3.5 mm, λ = 7 mm, w = 1 mm, H = 50 μm, t = 100 μm, s = 0.5 mm. Dimensioning is consistent across the sensor geometries, with only the microchannel pattern varying.

for a system to react intelligently to its environment. Existing solutions for joint angle sensing rely on thin-films and fibers that are flexible but not soft or stretchable. Existing commercial products include Bi-Flex Sensors^{TM} (Images Scientific Instruments), Bend Sensor® (Flexpoint Sensor Systems), and Flexiforce® Sensors (Tekscan, Inc.). Other examples include an angular displacement sensor containing a thin-metal-film strain gage, which operates with 100-750 Ω resistance and is accurate to within 10° [7]. A capacitive finger angle position sensor has also been developed, which features a high resolution of 0.02° over the absolute measurement range of 180° [8].

Finger joint angles are also measured using fiber Bragg grating (FBG) strain sensors [9]. In [10], a superstructure fiber Bragg grating is used to simultaneously measure strain and curvature. Other Bragg grating sensors have demonstrated evolving levels of sophistication, such as the capability to determine bend direction [11], [12], [13], integration of flexible materials such as elastomers [14] and polymer optical fiber [15], self-alignment [16], simultaneous temperature measurement [17] and general increased sensitivity [18].

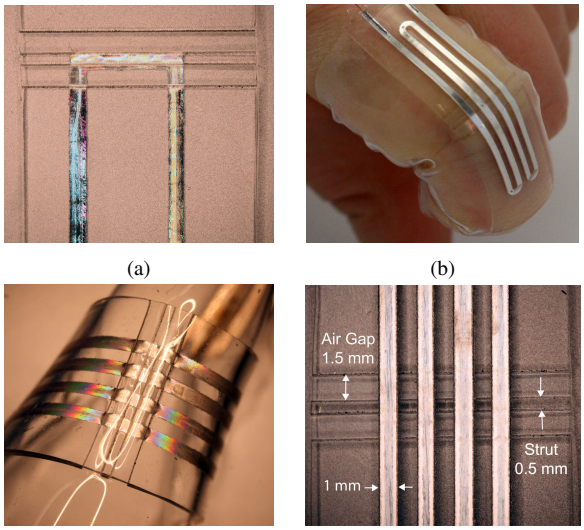

Fig. 4. Bend sensors for determining joint angles. (a) The pure curvature sensing geometry. (b) The combined strain-curvature sensor, made from a strain-sensing serpentine channel and including an integrated strut/gap layer. This device is further detailed in (c) and (d).

Despite high bend sensitivity, fiber Bragg gratings exhibit several disadvantages as curvature sensors, including measurement in reflection only or transmission only (for long-period gratings), broad resonant wavelengths that limit measurement accuracy, and strain-induced failure due to non-compliant materials. Strain or curvature sensors which are entirely soft would allow seamless integration into existing robotic manipulators, providing proprioceptive feedback with little or no interference to the motion of the system.

Existing bend sensors have been central in the development of data gloves for monitoring hand motion. An extensive review of glove-based motion acquisition is presented in [19]. Despite the enormous progress in this field, important challenges remain, including compliance matching with natural hand motion and active response for tactile feedback and motor assistance.

B. System Description

We combine stretch, pressure, and curvature sensing to introduce a family of wearable soft sensors that detect bending and joint position (Fig. 2), and that are composed of all-compliant elastomer and liquid materials. Three geometries are rigorously tested here: a curvature sensor, a strain sensor, and a combined strain and curvature sensor. The curvature sensor, shown in Fig. 2(a-b) and Fig. 4(a), measures direct curvature but is insensitive to strain. The strain sensor, seen in the inset of Fig. 1(a) and Fig. 2(d), measures differential strain but does not measure direct curvature. However, during finger bending, a sensor that is roughly adhered to the skin will both stretch around the knuckle as well as bend. Further-

more, the knuckle itself may apply pressure to the sensor's embedded microchannel during bending, hence increasing the measured change in resistance. We therefore test a third combined strain-curvature sensor, shown in Fig. 2(c) and Fig. 4(b-d). These sensors are composed of sub-millimeter thick films of polydimethylsiloxane (PDMS) rubber embedded with 50 μm deep channels of eGaIn conductive liquid.

In this particular study, the sensors are wrapped around a finger joint with the embedded sensing element positioned above the middle (second from the fingertip) knuckle. Bending the finger causes the knuckle to stretch the elastomer and exert a pressure on the sensing element. The combination of stretching, pressure, and curvature leads to a change ΔR in the electrical resistance of the sensor. Finger bending is detected when the relative change in resistance $r = \Delta R/R_0$ exceeds a critical threshold. The joint angle may also be estimated from the change in resistance, although this requires sensor calibration.

II. FABRICATION

A. Device Fabrication

Curvature sensors are produced through a combination of maskless photolithography, replica molding, and soft microfluidics manufacturing. Microchannel molds are fabricated by patterning kapton film on glass. 50 μm thick adhesive-backed polyimide film (McMaster-Carr) is adhered to clean glass slides (Electron Microscopy Sciences) and 1 mm wide microchannels are patterned with a laser micromachining system (VersaLaser, Universal Laser Systems). Excess kapton film is peeled away, and the pattern is rinsed with isopropyl alcohol and deionized water to remove residue. In order to discourage bonding between silicone rubber and the glass mold in subsequent steps, a hydrophobic monolayer is introduced to the glass surface through vapor deposition. The molds are placed in an evacuated chamber ($\sim$20 mTorr) with an open vessel containing a few drops of Trichloro(1H,1H,2H,2H-perfluorooctyl)silane (Aldrich) for at least 3 hours.

Patterning microchannels with kapton films presents a simple and fast fabrication method; however, these properties compromise edge definition and depth flexibility of the microchannels. To fabricate smaller channels (both in depth and width), photolithography techniques may be implemented.

PDMS (Sylgard 184, Dow Corning) is spin-coated in liquid form (10:1 mass ratio of elastomer base to curing agent) onto a mold, which results in a thin elastomer film of tunable thickness. An unpatterned film is also prepared by casting PDMS onto an unpatterned, silanized glass slide or silicon wafer. Each of the PDMS layers are cross-linked in the molds by oven-curing at $\sim 60\,^{\circ}$C for 30-40 minutes. Layers are manually removed from the molds and microchannels are constructed by bonding layers of patterned PDMS to unpatterned PDMS via oxygen plasma treatment (Technics Plasma Stripper/Cleaner; 65 W for 30 s).

The microchannels are filled by adhering small blocks of PDMS to the device inlet and outlet locations of the patterned elastomer film prior to removal from the mold. Small droplets of uncured silicone rubber are applied to the inlet and outlet locations, and blocks of PDMS (approximately 0.5 cm^3) are pressed into the droplets. The blocks are bonded to the elastomer film on a hotplate at 100$\,^{\circ}$C in approximately 20 minutes. Finally, holes are introduced into the blocks, providing an inlet and outlet for conventional tubing and syringe dispensing to fill the microchannels. Subsequently, the elastomer blocks are removed, the channels are wired, and openings are re-sealed with a final droplet of uncured PDMS. These final steps are enabled by the high surface energy of eGaIn, which allows a filled microchannel under no external pressure to remain intact even if the channel is not sealed.

The devices shown in Fig. 4 are composed of a 200 μm film of patterned PDMS bonded to a 100 μm film of unpatterned PDMS. These thicknesses correspond to a spin-coating speed of 380 rpm on glass and 730 rpm on silicon, respectively. The strut is fabricated by patterning two layers of 127 μm thick adhesive-backed kapton film on glass. In this work, the strut is laser-cut to be 0.5 mm in width and the gaps on either side of the strut are 1.5 mm in width. The strut is approximately 260 μm in height, and the final plate thickness is 300 μm. This structure (560 μm in total thickness) corresponds to a spin-coating speed of 183 rpm on glass. Note that these values have been achieved for one specific spin-coater, and it may be necessary to calibrate other machines to obtain similar results. The total thickness of the strain sensor is 300 μm, and the total thickness of the sensors with struts is 860 μm. Sensor dimensions are further detailed in Fig. 3.

B. Flexible Circuit Connections

Due to the low electric resistivity of eGaIn, the external wiring and electrical connections contribute significantly to both the total resistance of the eGaIn channel and resistance fluctuations. Motion of the wires that connect the liquid microchannels with the multimeter tends to cause considerable scatter during experimental testing. Therefore, an alternative technique has been developed in which a flexible circuit is bonded directly to one edge of the device, as shown in Fig. 5.

Flexible circuits are made from polyimide/copper laminate (DuPont). Circuit traces are achieved by patterning the copper via a photolithography process followed by a ferric chloride etch. Flexible circuits are bonded to PDMS films through an amino-epoxy chemical bonding method [20], [21]. First, an unpatterned PDMS surface is exposed to oxygen plasma (65 W for 30 s) and immediately coated in 5% (v/v) (3-Aminopropyl)triethoxysilane (99% Sigma Aldrich). The flexible circuit (polyimide film) is also treated with plasma, and the entire film is submerged in 5% (v/v) (3-Glycidyloxypropyl)trimethoxysilane (98% Sigma Aldrich). After at least 20 minutes, excess silane is discarded, the surfaces are rinsed with deionized water, and the films are placed on a hot plate or in an oven at 60$\,^{\circ}$C to dry. The unpatterned surface of the polyimide may then be bonded to the PDMS with light pressure. The same process is then repeated between the composite surface and a third layer of

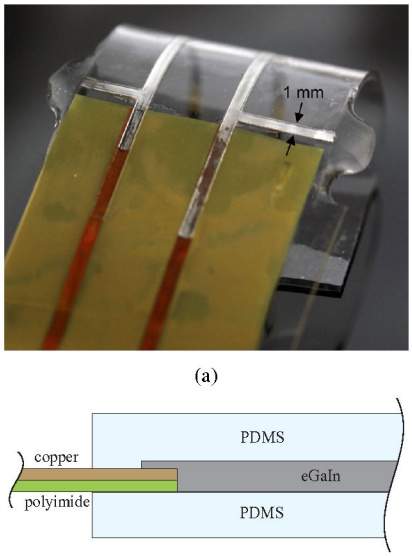

Fig. 5. (a) A patterned copper-polyimide film is bonded directly to one edge of a curvature sensor. The eGaIn-filled microchannel partially overlaps copper leads, which continue out of the microchannel and may be connected to external circuitry. (b) A cross-sectional view of the flexible circuit connection.

patterned PDMS. Placing the contacted surfaces in an oven at 60°C for several hours finalizes the chemical bond. In this final process, the copper leads of the flexible circuit must be carefully aligned with the inlet and outlet of the microchannel when bringing the surfaces into contact.

The contact resistance of the sensors does not noticeably change as a result of this electrical connection method.

III. CALIBRATION

The pure curvature sensor design was previously reported in [6], which also details a theoretical model for estimating change in resistance of the conductive liquid as a function of system curvature. As a general conclusion, ΔR demonstrates a quadratic dependence on θ for small bending curvatures (when the bending angle is small enough to apply the small angle approximation). For moderate or higher bending angles, the fit is more consistent with an exponential curve. However, this model breaks down under several conditions. A very thin (sub-millimeter) system will encounter enhanced boundary effects that cannot be accounted for in the predictive model. In addition, for a sensor that is thin and/or very soft, the inner plate is loaded under combined axial stress and moments during bending, which may result in plate buckling. If the inner plate buckles enough to contact the outer plate in the gaps, compressive force is distributed away from the strut, therefore disrupting the amount of pressure on the microchannel. Finally, a slight misalignment between the strut and embedded microchannel will reduce the pressure exerted on the channel. In this work, predictive models are not sufficiently accurate due to the scale and materials of the sensors. We therefore calibrate the sensor geometries to establish range and sensitivity.

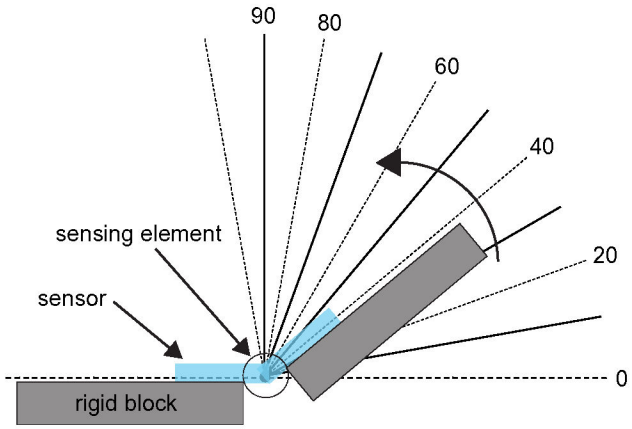

Fig. 6. Idealized calibration schematic.

A. Idealized Calibration

Curvature sensors were calibrated both on and off of a finger. Pure bending of the sensors was induced off of a finger by adhering the faces to rigid blocks and positioning the blocks at various angles, defined by an 'angle wheel' (Fig. 6). The edges of the blocks were carefully aligned with the edges of the curvature sensor gaps, separated by a distance $L = 3.5$ mm, such that all bending was concentrated at the location of the sensing element. When testing the strain sensor, the distance between the blocks remained consistent. The use of rigid blocks increases positioning accuracy, reduces twisting or stretching of the sensor and maintains the radius of curvature throughout testing.

The rigid blocks were oriented from 0° to 100°, at 10° increments, and the change in electrical resistance was measured with a precision multimeter (Agilent 34401A). Curvature measurements were repeated eight times for each sensor geometry, and are shown in Fig. 7(a). As expected, the change in electrical resistance ΔR increases as a function of bending angle θ. Green markers represent the strain sensor, black markers correspond to the pure curvature sensor, and red markers indicate the integrated geometry.

In this experimental setup, the pure curvature sensor demonstrates the greatest relative change in resistance during bending, which is expected given the pure bending condition. Between 0° and 90° the sensor's resistance increases on average by about 8% (0.82 Ω to 0.885 Ω, nominally), while the integrated strain-curvature sensor increases by about 3% (1.1 Ω to 1.14 Ω, nominally). This is intuitive, given that the length of the channel deformed in the curvature sensor is greater than the cumulative length of the channel deformed in the combined strain-curvature sensor. In the combined geometry sensor, the strut is 0.5 mm in width and intersects the 1 mm wide channel at four discrete locations, resulting in an area of intersection between the strut and channel of 2 mm^2. In the pure curvature sensor, the strut intersects the entire length of the channel that it is aligned with, which in this case is 7 mm in length. Hence, the area of intersection for

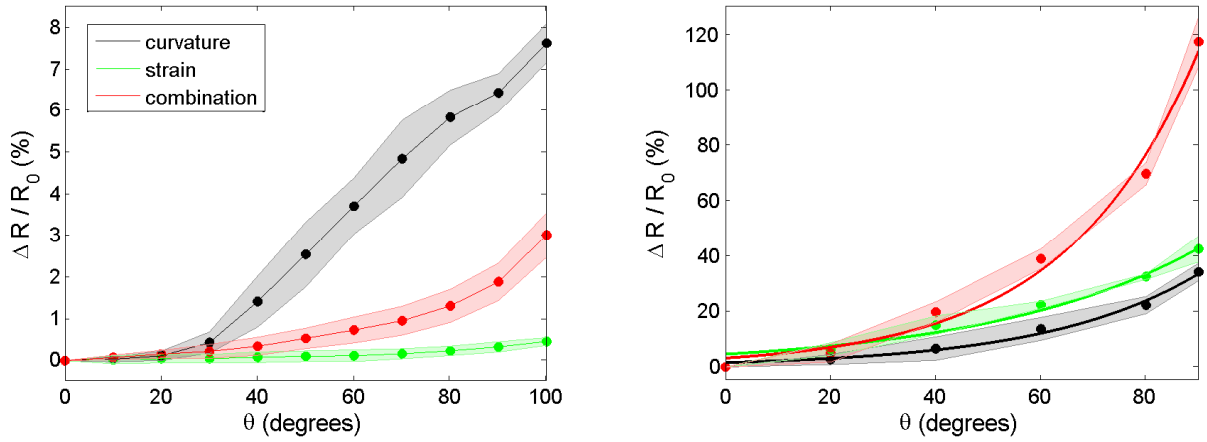

Fig. 7. Calibration curves for three sensor geometries taken (a) independently of a host and (b) when mounted on a host finger. Green, black and red markers correspond to the strain sensor, curvature sensor and integrated geometry, respectively. Shaded error bars represent one standard deviation of the data. On-finger calibrations were conducted only in the configuration for which the layer containing the microchannel is in contact with the finger. Percent change in resistance is calculated based on the R_0 values given in Table I and is a function of channel geometry.

this sensor is 3.5 mm^2. The pure curvature sensor is therefore more sensitive under the given testing condition. Predictably, the pure strain sensor does not display a notable change in resistance. As the sensor is only 300 μm in thickness, differential strain is minimal in this condition.

B. Finger-Mounted Calibration

Each sensor geometry was also calibrated and tested on a host finger. The sensor was wrapped around the index finger with the sensing element placed above the middle knuckle. Sensors with struts were worn such that the film containing the microchannel was in contact with the skin. The base electrical resistance was determined by keeping the finger straight. The finger was then positioned at bending angles between 0° and 90°, and the change in resistance was recorded. The finger joint was orientated using the same calibration setup (angle wheel) as in the idealized case, shown in Fig. 6. Lines of the 'angle wheel' were aligned with the top surface of the finger. Finger-mounted curvature measurements were repeated five times for each sensor geometry, and are shown in Fig. 7(b). The base resistance and the magnitude of the resistance change appear to be consistent for each sample tested. It is important to note that the exact relative change in resistance is not significant, as it should differ due to differences in the topology of the host manipulator or human finger. However, this analysis is useful in capturing general trends.

Interestingly, the combined strain-curvature sensor exhibits significantly enhanced sensitivity, especially as θ approaches 90°. The pure curvature sensor appears to be the least sensitive when integrated with a host finger, while the strain sensor seems to be slightly more sensitive than the curvature sensor. It is not immediately intuitive that the strain sensor should demonstrate this level of sensitivity. We hypothesize that the change in resistance observed is not due to differential strain, but rather that the knuckle exerts a pressure on the channels during bending, such that the channels are deformed locally around the knuckle as θ increases despite the absence of a strut. Thus, resistance across the channel increases exponentially with θ as increasing pressure is applied to the sensor. This effect applies to each of the geometries, and is supported by the order-of-magnitude increase in the scale of ΔR in Figures 7(a-b).

Exponential curves were fit to the data collected and are plotted in Fig. 7(b). Data fitting was achieved using the MATLAB Curve Fitting Tool (*cftool*). Because it is known that ΔR is zero when θ is zero, the curves are manually adjusted to intersect the origin. That is, for a curve fitted in the form $\Delta R = Ae^{b\theta}$, the y-intercept is known to be A and the final fit is taken to be $\Delta R = A(e^{b\theta} - 1)$. Therefore, we find that:

$$\theta = \frac{1}{b} log\left(\frac{\Delta R + A}{A}\right). \quad (1)$$

This manual adjustment is necessary to avoid the term within the logarithm of Equ. (1) evaluating to less than 1, resulting in negative finger joint angle values.

IV. EXPERIMENT

The electrical response of the wearable sensors is measured with a precision multimeter (Fluke 8845A) and recorded through a software interface (Flukeview Forms Basic). Video capture of finger movement is simultaneously recorded. During testing, a finger-cot (Qualatex XC) is worn over the host finger and sensor to maintain a close fit. Small markers (MoCap Solutions) are placed strategically on the side of the finger at the knuckle and each end of the bending joint. Video is subsequently analyzed with ProAnalyst (XCITEX motion analysis software), which tracks the three markers. Finally, relative marker positions are used to calculate finger joint angle throughout the testing period.

In each test, the finger bends to 90°, stays at 90° for a few seconds, and then straightens to 0°. Measurements are also taken for a rapid succession of bending and straightening, as well as partial bending (to approximately 45°). For sensor geometries containing a strut, the sensors are tested both with the layer containing the microchannel in contact with the finger and with the strut between the channel and finger.

V. RESULTS AND DISCUSSION

A plot of actual angle and predicted angle is presented in Fig. 8 for a series of finger bending motions. Actual joint angle is calculated based on motion analysis of video capture, and predicted joint angle is calculated based on the calibration curves derived from Fig. 7(b) and Equ. (1). From the top, the plots correspond to (a) a serpentine channel, (b) a straight channel with a strut on top (the layer containing the microchannel is in contact with the finger), and (c) a serpentine channel with a strut on top. The cases for which the layer containing the strut is in contact with the finger were also tested, but the results are omitted here due to decreased sensitivity of these configurations (discussed below).

As seen in Fig. 8, predicted joint angles for the strain sensor tend to be over-estimated, while predicted joint angles for both the curvature and combined strain-curvature sensors appear to be roughly consistent with actual joint position. Table I displays the average (taken as root mean square) deviation of $\theta_{predicted}$ from θ_{actual} over the periods of motion shown in Fig. 8, as well as average error given as a percent of the full-scale output of 90°. Accuracy of the sensors is highly dependent on care taken during calibration. It should be noted that slight differences in the calibration curve may lead to drastic changes in joint angle prediction, predominately due to the nonlinear dependence of ΔR on θ. Error may also be induced by the y-intercept adjustment to the exponential curve during calibration curve fitting. Further explanation for discrepancies between actual and predicted angles may include error during motion tracking and analysis, as well as fluidic or viscoelastic changes in the sensor itself.

Raw resistance data can be used to analyze the various sensor geometries and their relative sensitivities. In all cases, the relative change in electrical resistance $r = \Delta R/R_0$ is significant as the joint goes from straight to 90° bending. In one set of tests, the serpentine channel (absent of a strut) increases from approximately 1.1 to 1.8 Ω. This corresponds to a relative increase of approximately r = 64%. A relative change of r = 40% (0.82 to 1.15 Ω) is observed for a sensor composed of two films, a strut, and a straight channel when the film containing the channel is in contact with the skin. Interestingly, the sensor is less sensitive when the film containing the sensor is on the outside. In this case, the resistance increases from 0.82 to 0.9 Ω, and so r is only 10%.

The greatest sensitivity is measured with a sensor that contains both the strut and serpentine geometry, which is consistent with the calibration results. When the film containing the microchannel is in contact with the skin,

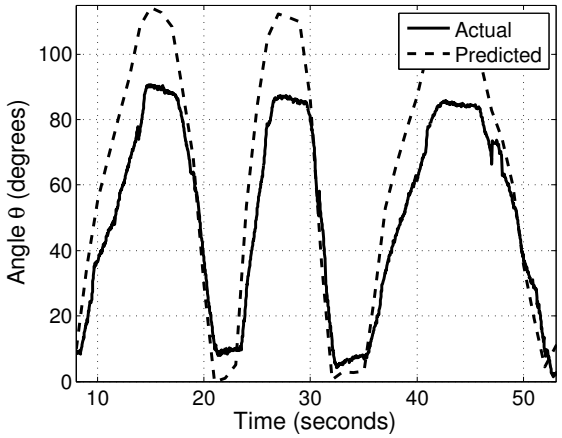

(a) - Strain Sensor

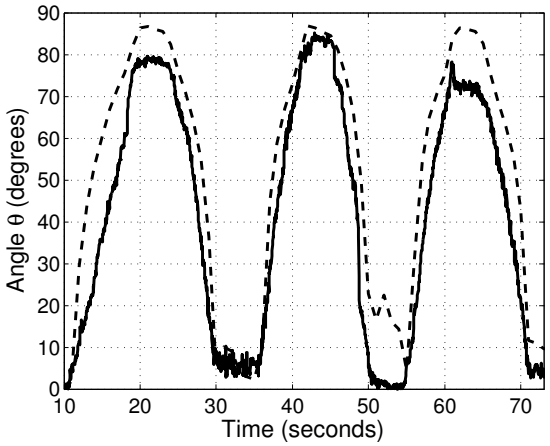

(b) - Curvature Sensor

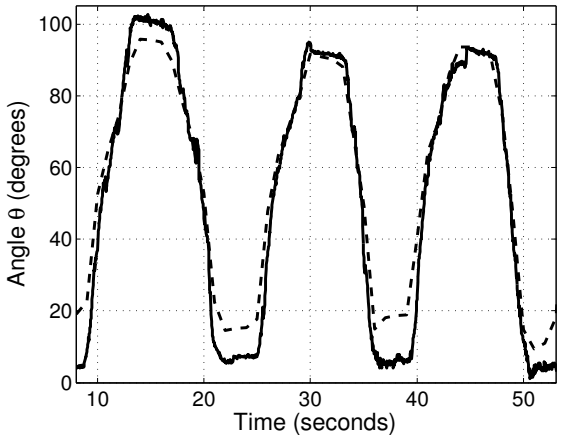

(c) - Combined Strain/Curvature Sensor

Fig. 8. Actual angle and predicted angle for a series of finger bending motions. From top: (a) Strain sensor geometry, composed of a simple serpentine channel embedded in an elastomer sheet. (b) Pure curvature sensor, composed of a straight channel and a strut. The layer containing the microchannel is in contact with the finger. (c) Combined strain-curvature sensor, composed of a serpentine channel and a strut. The layer containing the microchannel is in contact with the finger. Finger joint angles are predicted by the calibration curves derived in Fig. 7(b) and Equ. (1).

TABLE I

SUMMARY OF SENSOR PERFORMANCE

	R_0 (Ω)	$R_0 + \Delta R$ @ 90° bend (Ω)	$r = \Delta R/R_0$	RMS $\theta_{actual} - \theta_{predicted}$	RMS % error
Strain Sensor	1.1	1.8	64%	18.79°	20.87%
Curvature Sensor (eGaIn-side down)	0.82	1.15	40%	13.75°	15.28%
Combined Sensor (eGaIn-side down)	1.1	2.5	127%	7.94°	8.82%
Curvature Sensor (eGaIn-side up)	0.82	0.9	10%	—	—
Combined Sensor (eGaIn-side up)	1.1	1.4	27%	—	—

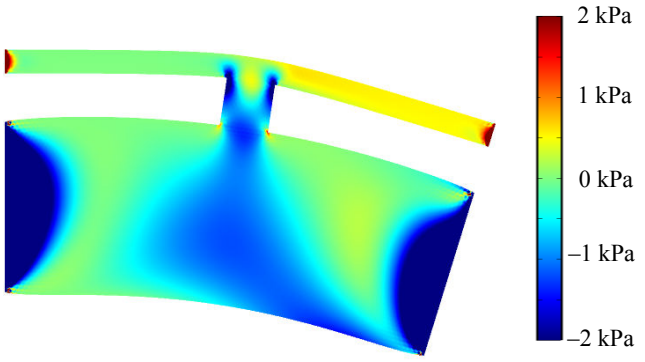

Fig. 9. Finite element analysis (COMSOL) of pressure distribution in the curvature sensing device when loaded onto a finger. The inner film has a thicker backing in order to simulate contact with the finger. In this simulation, the sensor has an elastic modulus of 167 kPa, a Poisson's ratio of 0.45, a strut width of 2 mm, a gap height of 2 mm, and inner and outer plate thicknesses of 7 mm and 1 mm, respectively. The stress on the outer (thinner) film is concentrated at the corners of the junction and away from the center of the junction. The stress on the inner (thicker) film is distributed uniformly throughout the junction, including at the center where the microchannel would be embedded. This is consistent with results demonstrating increased sensor sensitivity when the film containing the microchannel is in contact with the finger.

the resistance increases from 1.1 to 2.5 Ω and r = 127%. When the film containing the channel is on the outside, the resistance only increases to 1.4 Ω and r = 27%. These results are summarized in Table I.

According to these measurements, the strut only appears to be effective when it is above the microchannel (i.e. the film containing the microchannel is in contact with the skin). Because the channel is small relative to the size of the strut, its position should have no influence on the compressive force exerted by the strut during bending. The only factor that changes is the way that this compressive force is distributed around the embedded channel. As demonstrated by the finite element analysis (COMSOL 4.0) presented in Fig. 9, the stress on the outer film is concentrated at the corners of the junction and away from the center of the junction. In contrast, the stress on the inner film is distributed uniformly throughout the junction, including at the center where the microchannel would be embedded. In this analysis, the inner film has a thicker backing in order to simulate contact with the finger.

Alternatively, the sensors may be implemented as a binary switch, for which joint bending is detected when the relative change in resistance $r = \Delta R/R_0$ exceeds a critical threshold. This application eliminates the necessity for extensive sensor calibration.

VI. CONCLUSIONS AND FUTURE WORK

A curvature sensor composed of a thin elastomer film embedded with a microchannel of conductive liquid is presented. As a demonstration, the film is wrapped around a finger with the sensing element positioned on top of the knuckle. When the finger bends, the knuckle both stretches the elastomer and exerts pressure on the sensing element, leading to a change in the electrical resistance of the embedded conductive fluid-filled microchannel. In addition, an embedded pressure-exerting strut, which operates on principles of plate bending, enhances the resistance change and sensitivity of the sensor. The sensor is soft (elastic modulus $E \sim 1$ MPa) and stretchable (>350%) without losing functionality, and thus conforms to finger bending without restriction to the host. This sensor represents a flexible, stretchable and all-compliant solution for sensing bending angles, in contrast to many state-of-the-art technologies that feature rigid and motion restricting components. More classical rigid sensors may yield more accurate angle predictions, but at the expense of interference with the host.

Three geometries are explored in detail to distinguish the mechanics of strain sensing, curvature sensing, and combined strain-curvature sensing. These geometries are calibrated and tested both on and off of a finger, and the implications of the geometries have been discussed. The sensors exhibit an exponential relationship between bending angle and change in resistance. Multiple sensor geometries are evaluated and the results indicate that all designs are viable for joint angle proprioception, with the most appropriate depending on the host and application.

Sensor sensitivity may be increased by further optimizing the parameters of the design. Mainly, a reduction in microchannel aspect ratio (decreasing H and increasing w), a decrease in the layer thickness between the strut and the microchannel (decreasing t), and implementation of different materials may all increase sensor performance.

The compliant sensors and fabrication technology used in this study may serve many functions in robotic electronics and sensing. For example, the sensors presented here may be applied to robotic hands for both monitoring hand movements and tactile sensing for object manipulation. Future efforts may be focused on further integration of

hyperelastic pressure and curvature sensors with soft robots, artificial skin, integrated circuitry, and shape-mapping elastomer sheets.

VII. ACKNOWLEDGMENTS

This work is partially supported by the National Science Foundation (award number DMR-0820484) and the Wyss Institute for Biologically Inspired Engineering. Any opinions, findings and conclusions or recommendations expressed in this material are those of the authors and do not necessarily reflect those of the National Science Foundation. The authors thank Ben Finio for insightful discussions.

REFERENCES

[1] M. D. Dickey, R. C. Chiechi, R. J. Larsen, E. A. Weiss, D. A. Weitz, and G. M. Whitesides, "Eutectic gallium-indium (EGaIn): A liquid metal alloy for the formation of stable structures in microchannels at room temperature," *Adv. Funct. Mater.*, vol. 18, pp. 1097–1104, 2008.

[2] J.-H. So, J. Thelen, A. Qusba, G. J. Hayes, G. Lazzi, and M. D. Dickey, "Reversibly deformable and mechanically tunable fluidic antennas," *Adv. Funct. Mater.*, vol. 18, pp. 1097–1104, 2008.

[3] H.-J. Kim, C. Son, and B. Ziaie, "A multiaxial stretchable interconnect using liquid-alloy-filled elastomeric microchannels," *Appl. Phys. Lett.*, vol. 92, p. 011904, 2008.

[4] Y. L. Park, C. Majidi, R. Kramer, P. Berard, and R. J. Wood, "Silicone elastomer embedded with conductive liquid microchannels for hyperelastic pressure sensing," *Journal of Micromechanics and Microengineering*, vol. 20, p. 125029, 2010.

[5] R. Kramer, C. Majidi, and R. J. Wood, "Wearable tactile keypad with stretchable artificial skin," in *Proc. IEEE International Conference on Robotics and Automation (ICRA '11)*, Shanghai, China, May 2011.

[6] C. Majidi, R. Kramer, and R. J. Wood, "Non-Differential Elastomer Curvature Sensor for Softer-than-Skin Electronics," *Smart Materials & Structures (under review)*, 2011.

[7] E. Jesperson and M. Neuman, "A thin film strain gauge angular displacement sensor for measuring finger joint angles," in *Engineering in Medicine and Biology Society, 1988. Proceedings of the Annual International Conference of the IEEE*. IEEE, 2006, pp. 807–vol.

[8] G. Brasseur, "A capacitive finger-type angular-position and angular-speed sensor," in *Instrumentation and Measurement Technology Conference, 1998. IMTC/98. Conference Proceedings. IEEE*, vol. 2. IEEE, 1998, pp. 967–972.

[9] Y. Liu, L. Zhang, J. Williams, and I. Bennion, "Long-period fibre grating bend sensor based on measurement of resonance mode splitting," in *Lasers and Electro-Optics, 2000.(CLEO 2000). Conference on*. IEEE, 2000, pp. 306–307.

[10] B. Gwandu, X. Shu, Y. Liu, W. Zhang, L. Zhang, and I. Bennion, "Simultaneous measurement of strain and curvature using superstructure fibre Bragg gratings," *Sensors and Actuators A: Physical*, vol. 96, no. 2-3, pp. 133–139, 2002.

[11] Y. Wang and Y. Rao, "A novel long period fiber grating sensor measuring curvature and determining bend-direction simultaneously," *Sensors Journal, IEEE*, vol. 5, no. 5, pp. 839–843, 2005.

[12] L. Shao, L. Xiong, C. Chen, A. Laronche, and J. Albert, "Directional Bend Sensor Based on Re-Grown Tilted Fiber Bragg Grating," *Lightwave Technology, Journal of*, vol. 28, no. 18, pp. 2681–2687, 2010.

[13] T. Allsop, M. Dubov, A. Martinez, F. Floreani, I. Khrushchev, D. Webb, and I. Bennion, "Directional bend sensor based on an asymmetric modification of the fiber cladding by femtosecond laser," in *Conference on Lasers and Electro-Optics*. Optical Society of America, 2005.

[14] G. Kanellos, G. Papaioannou, D. Tsiokos, C. Mitrogiannis, G. Nianios, and N. Pleros, "Two dimensional polymer-embedded quasi-distributed FBG pressure sensor for biomedical applications," *Opt. Express*, vol. 18, pp. 179–186, 2010.

[15] X. Chen, C. Zhang, D. Webb, K. Kalli, and G. Peng, "Highly Sensitive Bend Sensor Based on Bragg Grating in Eccentric Core Polymer Fiber," *Photonics Technology Letters, IEEE*, vol. 22, no. 11, pp. 850–852, 2010.

[16] H. Patrick, "Self-aligning bipolar bend transducer based on long period grating written in eccentric core fibre," *Electronics Letters*, vol. 36, no. 21, pp. 1763–1764, 2000.

[17] C. Ye, S. James, and R. Tatam, "Simultaneous temperature and bend sensing with long-period fiber gratings," *Optics Letters*, vol. 25, no. 14, pp. 1007–1009, 2000.

[18] D. Zhao, K. Zhou, X. Chen, L. Zhang, I. Bennion, G. Flockhart, W. MacPherson, J. Barton, and J. Jones, "Implementation of vectorial bend sensors using long-period gratings UV-inscribed in special shape fibres," *Measurement Science and Technology*, vol. 15, p. 1647, 2004.

[19] L. Dipietro, A. Sabatini, and P. Dario, "A survey of glove-based systems and their applications," *Systems, Man, and Cybernetics, Part C: Applications and Reviews, IEEE Transactions on*, vol. 38, no. 4, pp. 461–482, 2008.

[20] M. Vlachopoulou, A. Tserepi, P. Pavli, P. Argitis, M. Sanopoulou, and K. Misiakos, "A low temperature surface modification assisted method for bonding plastic substrates," *Journal of Micromechanics and Microengineering*, vol. 19, p. 015007, 2009.

[21] L. Tang and N. Lee, "A facile route for irreversible bonding of plastic-PDMS hybrid microdevices at room temperature," *Lab Chip*, vol. 10, no. 10, pp. 1274–1280, 2010.